Wearable MXene Bioelectronics for Achilles Tendinopathy Diagnostics and Rehabilitation

Manini Rana (The University of Texas at Austin, Biomedical Engineering), *SUNFEST Fellow*
Dr. Raghav Garg, Ph.D., Department of Neurology, The University of Pennsylvania
Dr. Flavia Vitale, Ph.D., Department of Neurology, The University of Pennsylvania

***Abstract*— The Achilles tendon plays a crucial role in enabling multiple types of dynamic movement; however, as one of the most fragile structures in the body, its injury is extremely common. Acting in conjunction with multiple muscles, successful recovery of the Achilles tendon requires continuous monitoring of the loads that these muscles are imparting on it to avoid further detriment. To provide this insight, a novel application of MXene-based high-density surface electromyography (HD-sEMG) was innovated to capture muscle activation at specific points in the posterior lower leg. Spatial maps were generated to compare muscle activation across various activities and infer the resulting stress being placed on the Achilles tendon. The comfort, customizability, and high detail afforded by the investigated arrays propounds their future application in restorative physical therapy for tendinopathy patients, as well as in healing processes of other muscle groups and injuries.**

***Index Terms*— electromyography (EMG), high-density surface EMG, MXene, tendinopathy, radiography, ultrasound, impedance, Electrochemical Impedance Spectroscopy (EIS)**

I. Introduction

The Achilles tendon serves as one of the most critical facilitators of all types of motor movements that drive everyday life, yet is also one of the easiest to overburden or injure. Patients affected by Achilles tendinopathy, which refers to the various pathological changes that reduce the functionality of the Achilles tendon, may face resulting chronic pain, high recurrence rates, and continual impairments in their ability to walk, run, or move in other ways [1]. Furthermore, much of the persistent nature of Achilles tendinopathy stems from fear of further injury: to avoid consequent damage or rupture of the tendon, patients refrain from participating in sufficient physical activity, thus leading to deconditioning or even musculoskeletal atrophy [1]. Successful recovery from Achilles tendinopathy requires extensive physical therapy, during which clinicians should ideally be able to track the physiology and structure of the tendon to monitor progress. Many of the difficulties faced in successful restoration of the Achilles tendon, therefore, arise from a lack of information regarding patterns of muscle activation in different motor movements and their resulting loads in the lower calf and ankle areas. The majority of imaging and sensing technology employed in treating Achilles tendinopathy consists of (a) diagnostic radiography, ultrasonography, and MRI modalities [2], and (b) relatively novel electromyography (EMG) techniques measuring heterogeneity across muscle activation in dynamic tasks [3]. However, while these imaging systems provide excellent accuracy in tendinopathy diagnostic assessments [2], their inability to capture continuous motion hinders their usefulness in assessing tendon strain through stages of movement. Similarly, current EMG designs face limitations as well; the larger electrodes and bipolar designs utilized are insufficient in accounting for the large variability of muscle activity across the lower leg region [4]. To improve the range and precision of current EMG systems, a high-density surface EMG (HDsEMG) can be used to map specific muscle activation in the calf and give insight into the strain undertaken by the Achilles tendon across various movements.

This investigation draws upon the technology pioneered by Driscoll et al. in developing flexible, gel-free HDsEMG arrays composed of MXene electrodes that were successfully found to discriminate between areas of muscle activity within small muscle groups. Characterized by high skin-conformability, low impedance, and high electronic conductivity [6], MXenes yield high-resolution wearable sensors that are also patient-customizable [5, 7]. The HDsEMG array used in this study consists of 78 $Ti_3C_2T_x$ MXene electrodes spanning the medial and lateral gastrocnemius (24 electrodes on each) and lower soleus (30 electrodes) muscles. EMG voltages are recorded and processed using the wireless Ripple Grapevine Neural Interface Processor. This is the first application of HDsEMG in characterizing muscle activation surrounding the Achilles tendon. Trials conducted across patients with Achilles

tendinopathy during which spatial muscle activation is mapped for various exercises verify the efficacy of this technology. Successive analysis of these maps demonstrates how the spatial maps generated by HDsEMG can differentiate between specific activation patterns across the three calf muscles during each exercise, as well as how these activation patterns correspond to different degrees of Achilles tendon loading and strain in tendinopathy patients.

II. Background

A. Achilles Tendon Physiology

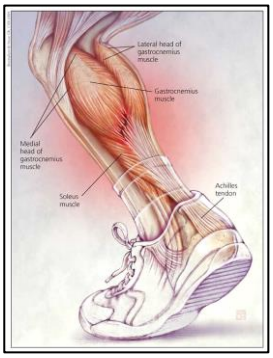

Fig. 1 *Diagram of the basic anatomy of the Achilles tendon. As shown, the gastrocnemius and soleus muscles are the primary muscles contributing to the activation of the tendon. Adapted from: Equilibrium Sports and Spinal Clinic.*

The location of the Achilles tendon, extending from mid-calf to just above the heel, enables it to act in conjunction with two primary calf muscles [8]. The gastrocnemius muscle is the first of these, composed of a medial and lateral head that join into a muscle belly in the posterior lower leg and fuse with the Achilles tendon near the middle of the calf [9, 10]. The muscle belly of the soleus, the second muscle investigated, is present behind the gastrocnemius. The two muscles merge to form the triceps surae along with the smaller plantaris muscle, and the conjoining of this muscle group to the Achilles tendon is what allows for the various types of ankle flexion [9].

Different motor tasks, ranging from basic ankle movements, such as dorsiflexion and plantarflexion, to compound ones, including heel raises, walking, and running, involve different activations of the gastrocnemius and soleus muscles. These movements generate stress on the Achilles tendon throughout their duration. While the gastrocnemius plays a greater function in walking, running, and jumping [11], the soleus provides more stability to the foot for standing [12]. Observation into muscle activation patterns for various types of movement can generate insight into which activities produce the greatest strain on the tendon and should therefore be monitored more delicately during the healing process.

B. Current Tendinopathy Imaging Modalities

While imaging technologies such as radiography, ultrasonography, and MRI proffer different advantages in the assessment of the Achilles tendon, their capabilities are nonetheless limited in generating a real-time picture of the tendon throughout dynamic movement.

Currently, radiography is the most widely applied technique in imaging the Achilles tendon as it is one of the fastest and most accessible clinical technologies and provides information about both the tendon and surrounding bone [2]. Its superiority in capturing erosion and displacement in the proximal bones makes it a strong indicator of arthritis and ossification in the tendon [2]; however, a lack of soft tissue contrast prevents sufficient insight into any muscle interaction.

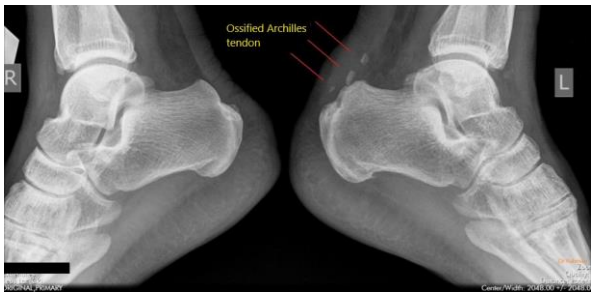

Fig. 2 *X-ray demonstrating calcified foci within the body of the Achilles tendon, along with a thickened soft tissue shadow. Both symptoms are consistent with diagnosis of Achilles tendinopathy. Adapted from: Dr. Abdul Rahman*

Modalities such as MRI and ultrasound are therefore also widely used due to their excellent soft tissue imaging abilities. While MRI is shown to provide high sensitivity in detecting abnormalities in tendinopathy patients with an accuracy of 89% [13], there have been several reports demonstrating similar MRI findings across symptomatic and asymptomatic tendinopathy patients, suggesting that MRI falls short in indicating the degree of tendinopathy present [14]. Ultrasound has similar benefits as MRI and is advantageous in that it is faster, more accessible, and has greater patient tolerability, but is limited by the training time and expertise required to operate it [2].

Fig. 3 *MRI (left) and ultrasound (right) images of the Achilles tendon. The MRI demonstrates a recurrent tear of the Achilles tendon, as well as fluid filling the tendon gap (arrows) in an 85-year old male patient. Adapted from: Radsource.*
The ultrasound captures a partial rupture of the Achilles tendon from subtendons of the gastrocnemius and soleus muscles. Adapted from: Szaro et. al., European Journal of Radiology., (2021)

While each of these modalities has unquestionable merit in diagnostics and staggered monitoring of Achilles tendinopathy, they are unable to provide sensitive and continuous data regarding the condition of the tendon in close stages of healing.

C. MXene-Based High Density Surface Electromyography

Electromyography offers a promising method of analyzing Achilles tendinopathy: rather than focusing on visual images of the tendon, it emphasizes the activity of the surrounding muscle, the strain being placed on the tendon, and verification as to whether motor movements are recuperating correctly after injury. With studies observing muscle activation patterns to be individual and task specific [3], current EMG systems face shortcomings due to their lack of customizability, specificity, and portability. Additionally, conventional electrodes at present require the use of an often abrasive gel to achieve an impedance level low enough to acquire a quality signal, which lends to patient discomfort [5].

MXenes, composed of transition metal carbides and nitrides, have been found to produce biocompatible films with high electronic conductivity and low impedance [5], presenting a promising option in creating a flexible and comfortable electrode array. MXene infused bioelectronic interfaces for high-density electrophysiology have been validated in the APB [7] and bicep muscles [5], with both electrode arrays demonstrating high skin conformability, high sEMG signal intensity, and muscle activation across specific areas.

Multiple factors can be customized to alter the characterization of MXenes used in these arrays, most notably concentration and flake size. The hydrophilic character of MXene [6] enables it to be diluted to its desired concentration through the addition of water; a more concentrated MXene will result in a more viscous, difficult-to-ink solution with greater conductivity, while a less concentrated MXene solution will be less conductive, but also thinner and easier to ink. MXene also comes in two flake sizes, large and small. During the fabrication process, the use of large flake MXene aids in increasing conductivity; however, small flake MXene is more versatile in the creation of smaller electrodes, especially at the nanoscale. Selecting the ideal concentration and flake size for each specific application of MXene may require extensive experimentation and testing but is critical for success.

III. Materials and Methods

This section discusses the materials and procedures used for ease of replication of these experiments and successive data analysis. This investigation was completed across four main steps: fabrication of MXtrode arrays, electrode characterization, patient trials, and spatial map generation.

A. Fabrication of MXtrode Arrays

Preparation of the MXtrode arrays was completed using an efficient, scalable procedure initially developed by Driscoll et. al. with modifications for the larger size of the gastrocnemius and soleus muscles. The schematic of the electrode arrays was designed on DraftSight and laser cut on a 55% cellulose and 45% polyester textile.

The MXtrode arrays were encapsulated by PDMS, a silicon-based organic polymer, on both sides to prevent textile degradation and tearing. The bottom layer was completed by preparing 15 g of PDMS in a 1:10 ratio of curing agent to base (to facilitate crosslinking) and was then spread onto a clean acrylic sheet in a very thin layer. Afterwards, PDMS was degassed to remove air bubbles and cured at 70°C for 30 minutes, resulting in a flexible and conformable film.

To adhere the laser cut textiles to the PDMS layer, Adapt medical bioadhesive was applied to the cured PDMS before placing the textile electrodes upon it. MXene was infused into the textiles by inking the fabric with a syringe. To ink the entirety of each 78-electrode calf array, approximately 20 mL of 20 mg/mL large-flake MXene was used. This concentration and flake size of MXene were found to yield the most favorable viscosity for efficient inking while also providing sufficiently low impedance and strong conductivity.

The inked electrodes were dried for 60 minutes at room temperature, followed by 30 minutes in a 25-30 mmHg pressurized vacuum oven at 70°C. 16-pin connectors were attached to each group of electrodes by screen printing conductive silver epoxy to the back ends, aligning each textile trace to its given channel on the connector, and cinching the connector shut. The silver epoxy was cured at 70°C for 90 minutes.

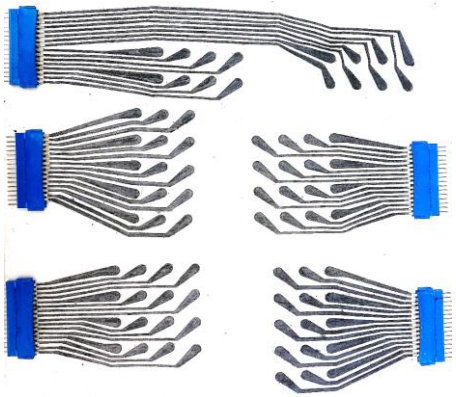

Fig. 4 *Setup of 78-MXtrode calf muscle array. 24 electrodes are to be placed on each the lateral and medial heads of the gastrocnemius muscle, with 30 across the entire soleus. At this point in the fabrication process, the electrodes would be conductive and ready for assembly via the blue connectors shown.*

The final passivation of the top surface of the MXtrodes was completed by preparing 30 g of 1:10 PDMS and spreading the solution over the arrays, ensuring all inked textile was completely covered. The encapsulated arrays were once again degassed for ten minutes to remove air bubbles and cured for one hour at 70°C.

Following the curing, the arrays were cut out of the excess surrounding PDMS. Using a 1 cm biopsy punch, circles of PDMS were cut out at the heads of the electrodes to expose the conductive MXene.

Fig. 5 *Close-up image of MXtrode heads after 1 cm biopsy punching. The lower stems of the MXtrode channels are seen to have a glossy sheen, illustrating the presence of the top PDMS encapsulation. The texture at the heads of the electrodes appears rougher as this is where the conductive textile is exposed for skin-interfacing.*

The MXtrode arrays were applicable for use after this stage of fabrication. While able to be used in any EMG system configuration, the setup designed for these studies was deliberately designed to provide a portable, wireless experience. To avoid extensive numbers of wires, printed circuit boards (PCBs) of 5.4 cm x 2.55 cm were designed to condense the electrode channels. Flex cables of customizable lengths were used to connect the MXtrode arrays to connectors soldered onto the PCBs and then to the Ripple Grapevine Neural Interface Processor, a wireless EMG voltage recording system. The utilization of these components allowed for a convenient system that enabled uninhibited motor movement of various types.

Fig. 6 *PCB soldered to connectors (left) and Ripple Grapevine Neural Interface Processor (right). Both components are integral in reducing the amount of wires used drastically. The connectors on the PCB chip snap directly into the blue connectors shown on the MXtrode array in Fig. 4. The Ripple system is connected to the rest of the device via flex cables and will report EMG readings using Bluetooth. Adapted from: Ripple.*

B. Electrode Characterization

For eventual applications in clinical settings, fabricated MXtrodes are required to match conventional electrodes in quality and performance. After the fabrication process detailed in the previous section, the Electrochemical Impedance Spectroscopy (EIS) of each electrode channel was measured using the Gamry Instruments DigiElch Electrochemical Simulation Software when placed in an electrochemical cell of 1 M NaCl phosphate-buffered saline. The heads of each MXtrode were submerged in this solution along with a standard Ag/Ag-Cl electrode to serve as the reference electrode. A pipette was used to remove the air bubbles, which would increase impedance, from the heads of the electrodes, and then the electrochemical cell was excited from frequencies of 1 Hz to 10^5 Hz. Graphs of the following design were generated to characterize the electrochemical impedance of the fabricated MXtrode arrays.

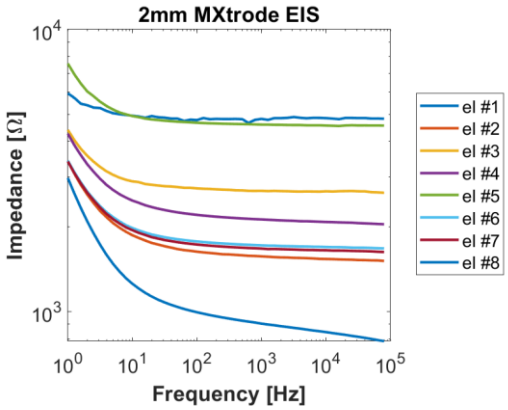

Fig. 7 *Electrochemical Impedance Spectroscopy graphs for a 2mm, 8 channel MXtrode array. Impedance* (Ω) *was measured for each channel continuously while increasing frequency* (Hz) *from 1 to* 10^5 *Hz. Each of the electrode channels is seen to follow a characteristically shaped curve, indicating consistent composition of the array.*

To provide a sufficient signal-to-noise ratio, the impedances for each electrode channel must fall under 1 $k\Omega$, which was not the case for the first series of EIS tests performed. A variety of factors may have influenced this result. To begin, the electrodes initially tested were significantly smaller at a 2 mm diameter in comparison to the final size of 1 cm, which would reduce the contact area between the electrode and electrochemical cell and increase impedance. Additionally, the MXene used was changed from a small-flake type to a large-flake one, which also lent a hand in reducing the impedance due to the increased overlap between the larger flakes. Following trials with these adjusted parameters, impedance readings across the electrodes for the same range of frequencies all fell below 1 $k\Omega$. This indicated that the fabricated MXtrodes met the standard to produce a sufficient signal-to-noise ratio (SNR).

C. *Patient Trials*

Upon validating the functionality of the fabricated MXtrodes, they were applied to healthy patients to determine their abilities in characterizing calf muscle activation across various movements. While the patients were instructed to complete many tasks, including plantar- and dorsi-flexion at different degrees, the main task of focus was calf raises. These were completed with toes facing inwards, outwards, and in a neutral stance.

Following skin preparation by swabbing the area with an alcohol wipe and gently abrading it, the arrays of 78 MXtrodes were placed onto the calves of ten subjects and then connected via the previously described method to the Ripple EMG measurement system. Each subject was instructed to complete ten calf raises (the neutral, toe in, and toe out calf raises were completed in separate trials) by applying the maximum voluntary force possible to contract their muscles at the peak of each calf raise. EMG voltage readings were taken across this time.

D. *Data Analysis and Spatial Map Generation*

In order to visualize the activation across the different areas of calf muscle, the data had to be converted from the raw electrode data to meaningful visual spatial maps. Using MATLAB, the EMG voltage readings for all electrodes were first band-pass filtered to remove noise from surroundings, RMS calculated, and then parsed through to manually delete channels with faulty data (flat reading or abnormally high values). The use of the high-density electrode system allowed for the removal of malfunctional channels without a significant amount of data loss.

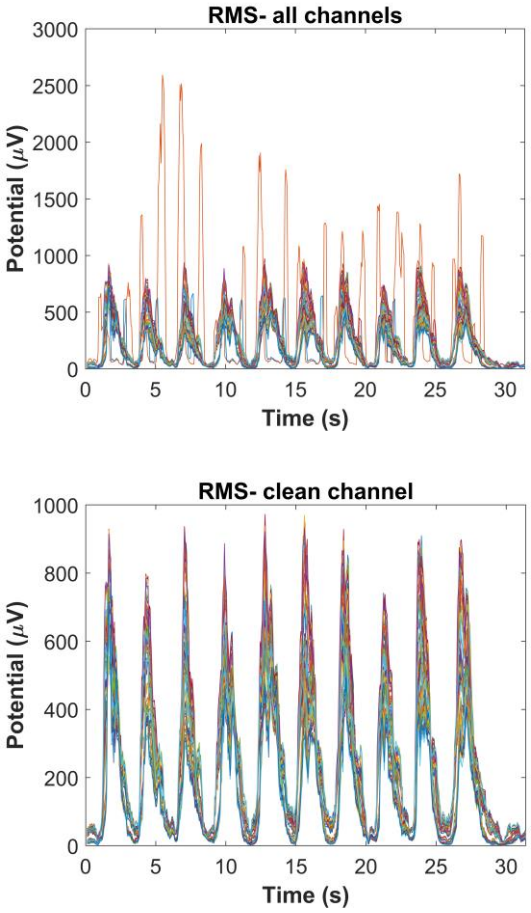

Fig. 8 *Unfiltered RMS data (top) and filtered RMS data (bottom) for a representative subject. Each colored line on the graphs represents an electrode channel. In the unfiltered data, faulty channels with inconsistently high readings or shifted time intervals can be seen. The cleaned data provides a more accurate picture about overall muscle activation patterns for normalization.*

Following filtration, the average maximum activation was found for each calf raise at the time when the majority of the electrode channels displayed maximum activation. The remaining electrode data was normalized with respect to this maximum, and then all channels were interpolated (to account for non-functional electrodes) for each muscle group to generate spatial maps of the activation.

In addition to visualizing spatial activation at the point of average maximum activation, another useful method of comparing the data was to calculate specific muscle activation volume for each type of calf raise. To compute this, spatial activation maps were generated at the maximum activation point for each of the ten calf raises, their volumes integrated for each muscle type, and the average volume calculated. This allows for direct comparison of how each activity is placing more or less load on a certain muscle group.

IV. Results and Discussion

To develop a system that is able to monitor calf muscle activation, and therefore predict loading on the Achilles tendon, the system would have to be precise enough to capture distinct differences in tendon loading across different regions of muscle. The robust character of the system in measuring muscle activation of patients in a convenient and accurate way had already been validated through completion of the study. Here, the spatial maps generated for a representative subject are discussed in the context of potential takeaways.

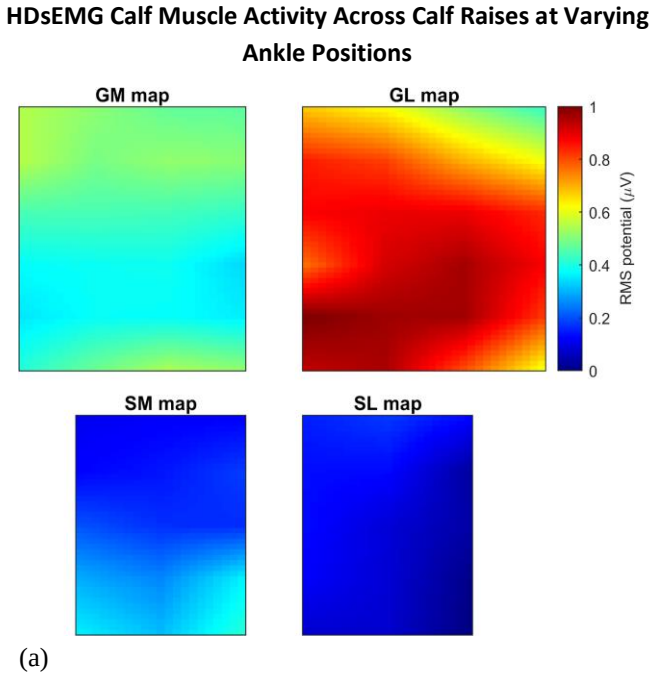

(a)

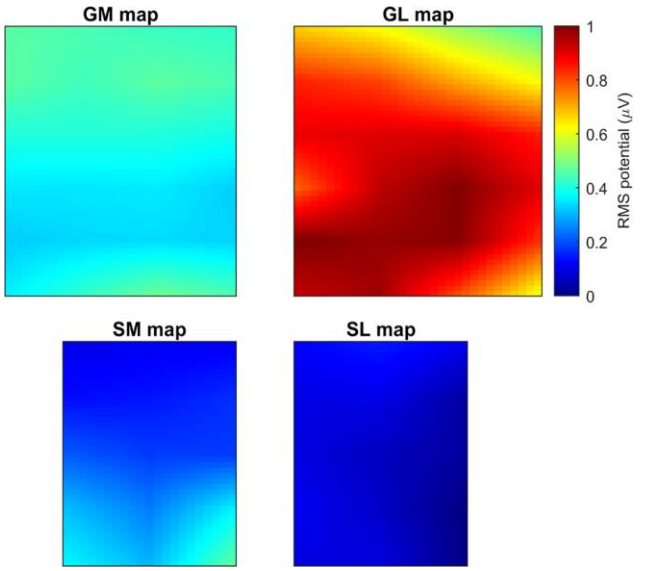

(b)

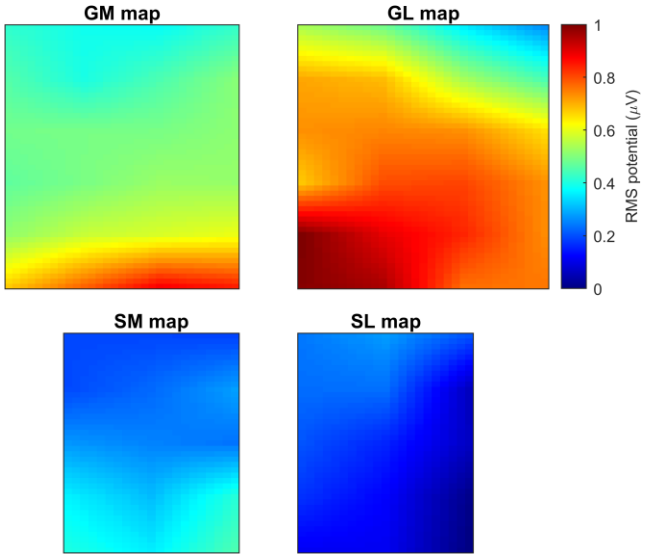

(c)

Fig. 9 *Spatial maps demonstrating high-density surface EMG results for calf muscle activity across calf raises at varying ankle positions: neutral (a), toe in (b), and toe out (c). The red areas on the maps corresponded to higher RMS potential readings, or higher activation, whereas blue signified points of lower activation.*

From each set of spatial maps generated for a subject, differences in muscle activation for each calf muscle group could be discerned. To begin, it was able to be determined that the lateral gastrocnemius underwent the greatest activation in calf raises exercises as compared to the remaining three muscle groups. Additionally, while muscle activation appeared almost entirely similar for the neutral and toe in calf raises, the toe out spatial map demonstrated reduced activation of the lateral gastrocnemius and slightly heightened activation of the medial gastrocnemius.

The ability of these spatial maps to distinguish between levels of activation across muscle groups confirms that they are

able to provide the desired level of detail to draw conclusions about force generated during patient movement. These spatial maps were able to translate minute differences in voltage from the EMG readings and display them in a manner that clearly distinguished muscle activation across different movements and locations.

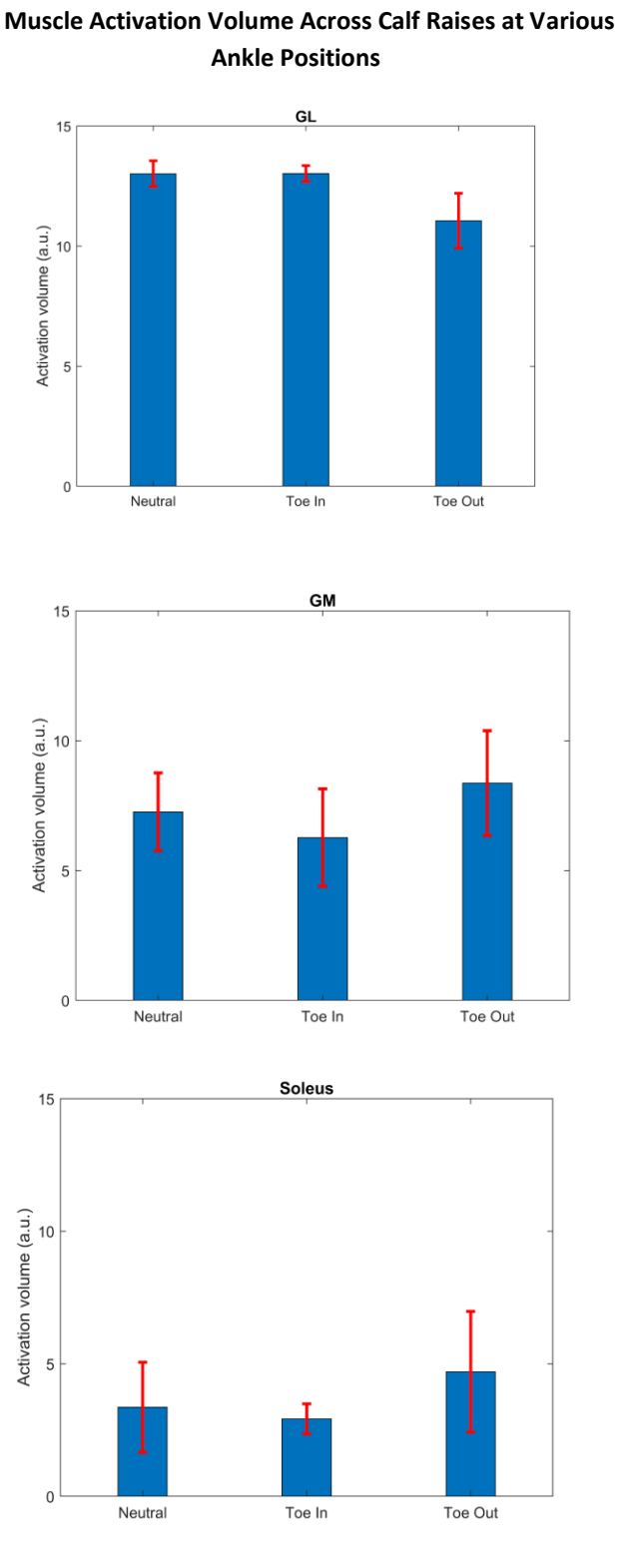

Fig. 10 *Bar graphs comparing mean activation volume for each muscle: lateral gastrocnemius (a), medial gastrocnemius (b), and soleus (c) for a representative subject. The red error bars represent standard deviation of the maximum activation volume across ten calf raises.*

To ensure that the system was distinguishing muscle activation at a statistically significant level that validated any recommendations made, bar graphs comparing muscle activation volume across the various activities were generated. While for this representative subject, muscle activation was not quite distinct enough to statistically differentiate between loading across each of the three activities, this model was able to present muscle activation differences in a quantifiable manner. Furthermore, in patients with Achilles tendinopathy, in which greater deviations across muscle activity are expected to be seen, this statistically-sound method of data visualization would elucidate important activation differences easily and accurately.

V. Conclusion and Future Directions

In this work, a design for a wearable MXene bioelectronic electrode array was developed in order to measure muscle activation across the calf and infer the resulting stress placed on the Achilles tendon. The fabrication process and comfort provided by MXene electrode arrays propounds their use as a gel-free, skin-conformable, and customizable option for capturing EMG measurements across calf muscles, as well as for future applications to other muscle groups in the body. The mapping of spatial activation across sections of calf muscles was able to demonstrate distinctions in muscle activity across various tasks with high specificity, providing great implications for physical therapy and restoration of the Achilles tendon.

Upon validation of this robust model of EMG analysis, future steps would include its utilization to discover potential muscle activation trends for different motor tasks, such as walking, running, and jumping. This would involve generating spatial maps for large numbers of healthy subject, to establish a baseline, and then conducting trials with patients with Achilles tendinopathy, successively.

For patients with tendinopathy, MXtrode arrays will reside inside a boot in conjunction with the wireless Ripple System to provide stability during healing. The technology developed to attach the MXtrode arrays in a portable and comfortable way to tendinopathy patients during trials will be ideally expanded to design a longer-term monitoring system for use in physical therapy and clinical offices, as well as an eventual at-home system. The portability and customizability of these MXtrode arrays enables clinicians to be able to track the physiology and structure of the tendon real time to monitor healing progress specific to individual patients. With this information, advice

can be imparted on adjusting the movement of each patient to reduce the loads being imparted on their tendon.

ACKNOWLEDGMENTS

The author would like to acknowledge the support of the National Science Foundation, through NSF REU grant no. 1950720. The author also thanks Dr. Flavia Vitale of the Department of Neurology at the University of Pennsylvania for the opportunity to research in her lab and for her support and guidance throughout this project. The author extends gratitude to Dr. Raghav Garg, also of the Department of Neurology at the University of Pennsylvania, for his invaluable mentorship and encouragement as well. Lastly, a special thanks to the Summer Undergraduate Fellowship in Sensor Technologies program at the University of Pennsylvania as well as the program coordinator Dr. Sue Ann Bidstrup Allen of the Department of Chemical and Biomolecular Engineering.

REFERENCES

[1] S. Mc Auliffe, A. Synott, H. Casey, K. Mc Creesh, H. Purtill, and K. O'Sullivan, "Beyond the tendon: Experiences and perceptions of people with persistent Achilles tendinopathy," *Musculoskelet. Sci. Pract.*, vol. 29, pp. 108–114, 2017, doi: 10.1016/j.msksp.2017.03.009.

[2] R. R. Bleakney and L. M. White, "Imaging of the achilles tendon," *Foot Ankle Clin.*, vol. 10, no. 2, pp. 239–254, 2005, doi: 10.1016/j.fcl.2005.01.006.

[3] N. J. Cronin, S. Kumpulainen, T. Joutjärvi, T. Finni, and H. Piitulainen, "Spatial variability of muscle activity during human walking: The effects of different EMG normalization approaches," *Neuroscience*, vol. 300, pp. 19–28, 2015, doi: 10.1016/j.neuroscience.2015.05.003.

[4] R. Merletti and S. Muceli, "Tutorial. Surface EMG detection in space and time: Best practices," *J. Electromyogr. Kinesiol.*, vol. 49, no. October, p. 102363, 2019, doi: 10.1016/j.jelekin.2019.102363.

[5] N. Driscoll *et al.*, "MXene-infused bioelectronic interfaces for multiscale electrophysiology and stimulation," *Sci. Transl. Med.*, vol. 13, no. 612, pp. 1–23, 2021, doi: 10.1126/scitranslmed.abf8629.

[6] A. VahidMohammadi, J. Rosen, and Y. Gogotsi, "The world of two-dimensional carbides and nitrides (MXenes)," *Science*, vol. 372, no. 6547, 2021, doi: 10.1126/science.abf1581.

[7] B. B. Murphy *et al.*, "A Gel-Free Ti3C2Tx-Based Electrode Array for High-Density, High-Resolution Surface Electromyography," *Adv. Mater. Technol.*, vol. 5, no. 8, pp. 1–10, 2020, doi: 10.1002/admt.202000325.

[8] M. N. Doral *et al.*, "Functional anatomy of the Achilles tendon," *Knee Surgery, Sport. Traumatol. Arthrosc.*, vol. 18, no. 5, pp. 638–643, May 2010, doi: 10.1007/s00167-010-1083-7.

[9] A. Del Buono, O. Chan, and N. Maffulli, "Achilles tendon: Functional anatomy and novel emerging models of imaging classification," *Int. Orthop.*, vol. 37, no. 4, pp. 715–721, 2013, doi: 10.1007/s00264-012-1743-y.

[10] Y. Watanabe *et al.*, "Functional anatomy of the posterolateral structures of the knee," *Arthrosc. J. Arthrosc. Relat. Surg.*, vol. 9, no. 1, pp. 57–62, Feb. 1993, doi: 10.1016/S0749-8063(05)80344-5.

[11] A. R. Fugl-Meyer, G. Nordin, M. Sjöström, and L. Wählby, "Achilles tendon injury. 5. A model of isokinetic strength training using biofeedback.," *Scand. J. Rehabil. Med.*, vol. 11, no. 1, pp. 37–44, 1979, [Online]. Available: http://www.ncbi.nlm.nih.gov/pubmed/419397.

[12] W. E. Garrett, J. C. Califf, and F. H. Bassett, "Histochemical correlates of hamstring injuries," *Am. J. Sports Med.*, vol. 12, no. 2, pp. 98–103, Mar. 1984, doi: 10.1177/036354658401200202.

[13] P. T. Karjalainen *et al.*, "MR Imaging of Overuse Injuries of the Achilles Tendon," *Am. J. Roentgenol.*, vol. 175, no. 1, pp. 251–260, Jul. 2000, doi: 10.2214/ajr.175.1.1750251.

[14] K. Soila, P. T. Karjalainen, H. J. Aronen, H. K. Pihlajamäki, and P. J. Tirman, "High-resolution MR imaging of the asymptomatic Achilles tendon: new observations.," *Am. J. Roentgenol.*, vol. 173, no. 2, pp. 323–328, Aug. 1999, doi: 10.2214/ajr.173.2.10430128.